Nuclear Medicine and Biology 43 (2016) 280–287

Contents lists available at ScienceDirect

Nuclear Medicine and Biology

journal homepage: www.elsevier.com/locate/nucmedbio

Labeling and preliminary *in vivo* assessment of niobium-labeled radioactive species: A proof-of-concept study

Valery Radchenko [a,*], Penelope Bouziotis [b], Theodoros Tsotakos [b], Mari Paravatou-Petsotas [b], Ana de la Fuente [a], George Loudos [b,c], Adrian L. Harris [d], Stavros Xanthopoulos [b], Dmitry Filosofov [e], Harald Hauser [f], Michael Eisenhut [f], Bernard Ponsard [g], Frank Roesch [a,**]

[a] Institute of Nuclear Chemistry, Johannes Gutenberg University, Mainz, Germany
[b] Institute of Nuclear & Radiological Sciences & Technology, Energy & Safety, N.C.S.R. "Demokritos", Athens, Greece
[c] Department of Biomedical Engineering, Technological Educational Institute of Athens, Athens, Greece
[d] Weatherall Institute of Molecular Medicine, University of Oxford, Oxford, UK
[e] Dzhelepov Laboratory of Nuclear Problems, Joint Institute of Nuclear Research, Dubna, Moscow region, Russian Federation
[f] Radiopharmaceutical Chemistry, German Cancer Research Center, Heidelberg, Germany
[g] Institute of Nuclear Materials Science, BR2 Reactor, Radioisotopes and NTD Silicon Production, Belgian Nuclear Research Centre, SCKCEN, Mol, Belgium

ARTICLE INFO

Article history:
Received 14 November 2015
Received in revised form 15 January 2016
Accepted 4 February 2016

Keywords:
$^{95/90}$Nb
Bevacizumab
Labeling
VEGFR
Biodistribution
PET imaging

ABSTRACT

The application of radionuclide-labeled biomolecules such as monoclonal antibodies or antibody fragments for imaging purposes is called *immunoscintigraphy*. More specifically, when the nuclides used are positron emitters, such as zirconium-89, the technique is referred to as *immuno-PET*. Currently, there is an urgent need for radionuclides with a half-life which correlates well with the biological kinetics of the biomolecules under question and which can be attached to the proteins by robust labeling chemistry. ^{90}Nb is a promising candidate for *in vivo immuno-PET*, due its half-life of 14.6 h and low β^+ energy of $E_{mean} = 0.35$ MeV per decay. ^{95}Nb on the other hand, is a convenient alternative for longer-term *ex vivo* biodistribution studies, due to its longer half-life of ($t½ = 35$ days) and its convenient, lower-cost production (reactor-based production).
In this proof-of-principle work, the monoclonal antibody bevacizumab (Avastin®) was labeled with $^{95/90}$Nb and *in vitro* and *in vivo* stability was evaluated in normal Swiss mice and in tumor-bearing SCID mice.
Initial *ex vivo* experiments with ^{95}Nb-bevacizumab showed adequate tumor uptake, however at the same time high uptake in the liver, spleen and kidneys was observed. In order to investigate whether this behavior is due to instability of *Nb-bevacizumab or to the creation of other *Nb species *in vivo*, we performed biodistribution studies of ^{95}Nb-oxalate, ^{95}Nb-chloride and ^{95}Nb-Df. These potential metabolite species did not show any specific uptake, apart from bone accumulation for ^{95}Nb-oxalate and ^{95}Nb-chloride, which, interestingly, may serve as an "indicator" for the release of ^{90}Nb from labeled biomolecules. Concerning the initial uptake of ^{95}Nb-bevacizumab in non-tumor tissue, biodistribution of a higher specific activity radiolabeled antibody sample did show only negligible uptake in the liver, spleen, kidneys or bones. *In-vivo* imaging of a tumor-bearing SCID mouse after injection with ^{90}Nb-bevacizumab was acquired on an experimental small-animal PET camera, and indeed showed localization of the radiotracer in the tumor area. It is the first time that such results are described in the literature, and indicates promise of application of ^{90}Nb-labeled antibodies for the purposes of *immuno*-PET.
Published by Elsevier Inc.

1. Introduction

Targeted imaging of cancer is crucial to modern-day cancer management, and radionuclides attached to biomolecules are an exciting strategy for tumor diagnosis and therapy [1]. An attractive feature, but also the key challenge of this strategy is to select radionuclides and targeting vehicles with characteristics which are best suited for a particular application.

Angiogenesis is the development of new blood vessels from pre-existing ones. Angiogenesis is regulated by chemical signals of the organism, which function as an "angiogenesis switch", regulating the formation of new vasculature. Bevacizumab is a humanized monoclonal antibody (mAb) which binds all VEGF-A isoforms [2]. Currently many studies focus on labeling of bevacizumab with radionuclides for *in vivo* evaluation [3–7]. An important criterion for selecting of radionuclides for mAb is the half-life of the radionuclide which should favorably correlate to the biological kinetic of large-size biomolecules. Due to the long circulation of intact antibodies, optimal tumor-to-non tumor ratios

* Corresponding author at: P.O. Box 1610, Los Alamos, New Mexico 87544, USA. Tel.: +1 5056672281; fax: +1 5056061801.
** Corresponding author.
E-mail addresses: varad@lanl.gov (V. Radchenko), frank.roesch@uni-mainz.de (F. Roesch).

http://dx.doi.org/10.1016/j.nucmedbio.2016.02.003
0969-8051/Published by Elsevier Inc.

can be reached from approximately 2 to 5 days post-injection. Therefore, radionuclides with an appropriate half-life should be chosen. Positron-emitting radionuclides with long and medium-long half-lives of interest for PET-imaging with antibodies and antibody fragments are, for example, ^{89}Zr ($t_{1/2}$ = 78.4 h) [8,9], ^{64}Cu ($t_{1/2}$ = 12.7 h) [10,11], ^{86}Y ($t_{1/2}$ = 14.7 h) [12], ^{76}Br ($t_{1/2}$ = 16.0 h) [13].

Several crucial factors and characteristics apply to radionuclide candidates for *immuno*-PET. The most important ones are: i) a physical half-life paralleling the biological half-life of the mAb or antibody fragment; ii) a high positron branching with no or weak accompanying other radiation (β^-, γ) to offer high-sensitivity PET imaging while reducing the radiation burden of the patient; iii) a preferably low β^+-energy to allow for high-resolution PET imaging; and iv) the availability of the radionuclide, i.e., an efficient production and radiochemical separation route.

In previous works we have reported a convenient way for production of ^{90}Nb–labeled biomolecules and proposed ^{90}Nb as a promising candidate for application in *immuno*-PET [14–17]. Its intermediate half-life of 14.6 h and a high positron branching of 53% may make ^{90}Nb an ideal candidate for application with antibody fragments, monoclonal antibodies, drug delivery systems and nanoparticles. Moreover, the chelate desferrioxamine has been identified as an excellent moiety to label *Nb to proteins [17,18].

In this work we report on the *in vitro* stability and *in vivo* behavior of $^{95/90}$Nb radiolabeled bevacizumab. Biodistribution studies of ^{95}Nb-oxalate, ^{95}Nb-chloride and ^{95}Nb-Df were performed in healthy mice, to provide more information on the fate of *Nb-labeled species *in vivo*.

2. Materials and methods

2.1. Materials

Reagents were purchased from Sigma-Aldrich (Germany) and used without further purification, unless otherwise stated. Deionized water (18 MΩ cm^{-1}) and ultra-pure HCl solution were used. No further special measures were taken regarding working under strict metal-free conditions. The mAb Bevacizumab (Avastin®, Roche) directed against the VEGF-A family of isoforms was bought from Roche Ellas S. A. (Greece). For the purification of conjugated and labeled antibodies, PD-10 columns (GE Healthcare Life Science) were applied, for ion exchange separation Aminex A27, 15 ± 2 μm and AG1x8, 200–400 mesh anionic exchange resins and DOWEX50x8, 200–400 mesh (BioRad) were used. For solid phase extraction, UTEVA® resin (Triskem Int., France) was applied.

The production yield, radionuclidic purity, radiochemical purity and separation yield of $^{95/90}$Nb were determined by γ-ray spectroscopy using an Ortec HPGe detector system and Canberra Genie 2000 software. The dead time of the detector was always kept below 10%. The detector was calibrated for efficiency at all positions with the certified standard solution QCY48, R6/50/38 (Amersham, UK).

VEGF165-transfected MDA MB 213 cells (M165) were kindly provided by Cancer Research UK. MDA MB 231 breast cancer cells were infected with virus expressing VEGF 165. The virus was made in Pheonix cells using the plasmid pLXRSpBMN-IRES-GFP. The VEGF clone is human. The cells are cultured at safety level I in minimum essential medium (Eagle) with 2 mM L-glutamine in the presence of 10% fetal bovine serum, at 37 °C in a humidified 5% CO_2 incubator.

Labeling efficiency and stability of the $^{95/90}$Nb labeled mAb was monitored by instant thin layer chromatography (iTLC) and high performance liquid chromatography (HPLC). ITLC was performed on chromatography strips (Biodex, NY). As mobile phase, 0.02 M citrate buffer (pH 5.0) was used. HPLC monitoring was performed on a Waters HPLC system using a TSKgel G3000SWXL size exclusion column (TOSOH Bioscience, Germany). As eluent, a mixture of 0.05 M sodium phosphate and 0.15 M sodium chloride (pH 6.8) solution was used at a flow rate of 0.8 mL/min.

Formation of ^{95}Nb-Df was measured *via* ITLC at conditions described above.

All numerical data were expressed as the mean of the values ± the standard error of the mean. Statistical analysis was performed using the t-test. A p value less than 0.05 was considered statistically significant.

2.2. Production of ^{90}Nb and ^{95}Nb

^{90}Nb was produced *via* the ^{90}Zr(p,n)^{90}Nb reaction at the cyclotron MC32NI of the German Cancer Research Center, Heidelberg. For irradiation, a stack of three disks of natural zirconium (natural abundance: 51.45% ^{90}Zr) foils of 10 mm diameter and a thickness of 0.25 mm each was used. Irradiation was performed at 20 MeV proton energy and a current of 5 μA for 1 h. This initial proton energy decreased, by using an aluminum holder cover of 0.5 mm thickness, to 17.5 MeV while entering the first foil of Zr. Twenty-four hours after end of irradiation (EOB), production yield and impurities were measured by gamma ray spectroscopy. The absolute activity of ^{90}Nb was calculated as average of its two gamma-lines at 141.2 keV (66.8% abundance) and 1129.2 keV (92.7%).

^{95}Nb ($t_{1/2}$ = 35 days) was employed for the *ex vitro* biodistribution experiments. ^{95}Nb was produced *via* the ^{94}Zr(n, γ) → ^{95}Zr(β^-, $t_{1/2}$ = 64 days) → ^{95}Nb reaction from natural zirconium granules (1–3 mm, 99.8% ChemPur, Germany). Neutron irradiations were performed at the BR2 reactor at the Belgian Nuclear Research Centre, Belgium and at BERII reactor at Helmholtz Centre in Berlin, Germany.

The production of the radionuclides ^{95}Zr/^{95}Nb and ^{90}Nb was monitored by gamma ray spectroscopy, *via* emissions at 724.2 keV (44.2%) and 756.7 keV (54.0%) for ^{95}Zr, and at 765.8 keV (100%) for ^{95}Nb and 1129 KeV (92%) for ^{90}Nb.

2.3. Separation and purification of n.c.a. $^{95/90}$Nb

2.3.1. First separation strategy

The first separation strategy was applied for biodistribution studies in tumor-bearing mice. The separation procedure was modified following the procedure described by Busse et al. [14]. In short, the zirconium metal target (260 ± 3 mg) was transferred into a 50 mL vial and 2 mL of water was added. Under ice-cooling, 48% HF (0.63 mL) was added in small portions. After complete dissolution, 10 M HCl (6 mL) and saturated boric acid (3.4 mL) were added. The $^{95/90}$Nb fraction was extracted with 0.02 M *N*-benzoyl-*N*-phenylhydroxylamine (BPHA) in $CHCl_3$ (5 mL) by vigorous stirring of the two phases in a 50 mL vial for 20 min. The aqueous phase was additionally washed with $CHCl_3$ (3 mL). The organic phases were combined and washed with a mixture of 9 M HCl/0.001 M HF (2 mL) and with 9 M HCl (2 mL) and finally extracted with aqua regia (5 mL).

For a final purification of $^{95/90}$Nb from remaining trace amounts of zirconium, an anionic exchange method was employed. After the aforementioned back extraction, the aqueous phase was evaporated to dryness. The residue was dissolved in a mixture of 0.25 M HCl/0.1 M oxalic acid (0.5 mL) and adsorbed onto a small Aminex A27 (15 ± 2 μm) anionic exchange column (20 × 1.5 mm). Elution was performed under slight overpressure of 0.3 bars. After loading, the column was washed with 10 M HCl (100 μL). Residues of Zr were removed by washing with a mixture of 9 M HCl/0.001 M HF (200 μL). $^{95/90}$Nb was eluted by a mixture of 6 M HCl/0.01 M oxalic acid (200 μL).

2.3.2. Alternative separation strategy

A second separation strategy was applied to provide a sample of ^{95}Nb with a higher radioactive concentration, for use in consequent biodistribution studies. Crude separation from the Zr target was applied following a published protocol [16]. In short, 2 mL of 21 M hydrofluoric acid containing the irradiated zirconium target was passed through the cation exchange resin (DOWEX 50 × 8, 100 mg, 200–400 mesh, 10 × 5

mm) resin in F^- form for the removal of colloids, unsolved target particles and possible trace contamination of 2+ and 3+ charged metal cations, such as for example Cu^{2+} or Fe^{3+}, from the target holder. The column was additionally washed with concentrated hydrofluoric acid (1 mL). The solution (3 mL) which passed through the cation exchange resin was transferred to an anion exchange column (300 mg, 25 × 5 mm) filled with AG 1 × 8 resin (200–400 mesh) in the F^- form. Nb^V remained on this resin and the bulk amount of Zr^{IV} passed through. The column was washed with concentrated HF (4.5 mL) to elute traces of Zr^{IV}, while *Nb stays on the column.

A small plastic column was filled with UTEVA resin (150 μm, 100 mg, 10 × 5 mm). The aforementioned anion exchange column was directly connected with the UTEVA column and 7 mL of 0.3 M oxalic acid/7.5 M HCl were passed through both columns.

The UTEVA column was next washed with 5 M HCl (5 mL). Traces of Zr^{IV} passed through the UTEVA, while $^*Nb^V$ remains absorbed on the column. For elution of *Nb 0.1 M oxalic acid was applied. The column was washed with 200 μL and *Nb eluted with another 400 μL of 0.1 M oxalic acid.

2.4. Preparation of ^{95}Nb-oxalate, ^{95}Nb-chloride, and ^{95}Nb-desferrioxamine (Df)

^{95}Nb-oxalate (10 mM) was prepared by dilution of the aliquot of the purified ^{95}Nb (5 ± 1 MBq) fraction with saline. ^{95}Nb-chloride was prepared by evaporation of an aliquot (50 μL) of the oxalate fraction obtained after ^{95}Nb (5 ± 1 MBq) purification and addition of several portions (3 × 100 μL) of 30% HCl, after which the mixture was the dried again at 100 °C. The resulting preparation was dissolved in saline. For the preparation of ^{95}Nb-Df, 50 mM of Df in saline (1.45 mL) was mixed with ^{95}Nb-oxalate (50 μL) and incubated for 30 min at room temperature. The formation of ^{95}Nb-Df was monitored by thin layer chromatography.

2.5. Monoclonal antibody modification with Df-Bz-NCS

The labeling of bevacizumab with ^{95}Nb was performed after the coupling of desferroxiamine to bevacizumab. Coupling was performed by use of the novel bifunctional chelator p-isothiocyanatobenzyl-desferroxiamine B (Df-Bz-NCS) from Macrocyclics (Dallas, USA). In short, while gently shaking, a threefold molar excess of Df-Bz-NCS (in 25 μL DMSO) was added to the mAb (2–3 mg in 1 mL 0.1 M $NaHCO_3$ buffer, pH 9.0), and incubated for 30 min at 37 °C. Non-conjugated chelate was removed by size-exclusion chromatography using a PD-10 column and 0.9% sodium chloride (pH 6.5) as the eluent. The number of chelates per antibody was assumed to be 1.5 according to our previous work [16] and the report from Perk et al. [18].

2.6. Labeling of bevacizumab with $^{95/90}$Nb

Df-Bz-NCS-bevacizumab was labeled with $^{95/90}$Nb following two different labeling protocols. For the first protocol, to a $^{95/90}$Nb solution (10 ± 2 MBq for ^{95}Nb) in 6 M HCl/0.01 M oxalic acid solution (200 μL), 6 M NaOH (180 μL) and 1 M NaOH (230 μL) were added. After 3 min, 0.5 M HEPES buffer (pH 7.0) (390 μL) and Df-Bz-NCS-mAb (1.5 mg/mL) (1.0 mL) were added. The total volume of the mixture was 2 mL.

For the second labeling protocol, a purified $^{95/90}$Nb fraction (10 ± 2 MBq for ^{95}Nb) in 0.1 M oxalic acid (20 μL) was mixed with 300 μL of normal saline and then the mixture was adjusted to pH 6–7 with 0.1 M Na_2CO_3 (50–60 μL). The modified mAb (300 μg, 2 nmol, 120 μL) was then added to this mixture and then the volume of the mixture was adjusted to 1 mL with normal saline. Both mixtures were incubated at room temperature for 60 min. Analysis of product formation was monitored by ITLC (0.02 M citric acid/MECN, 90/10) at 10, 30 and 60 min and by HPLC at 60 min post-incubation. Finally, $^{95/90}$Nb-Df-Bz-NCS-bevacizumab was purified by using a PD-10 column, with 0.9% sodium chloride solution as the mobile phase. Fig. 1 schematically represents Df-modification and *Nb labeling.

2.7. In vitro stability

Stability of $^{95/90}$Nb-bevacizumab was studied in two setups, first in normal saline at room temperature and in fresh human plasma at 37 °C. For preparation of human plasma, human blood was collected in heparinized polypropylene tubes and centrifuged at 5000 rpm at 4 °C for 5 min. The plasma was collected and three fold excess (300 μL) was incubated with $^{95/90}$Nb-Bevacizumab (100 μL) at 37 °C. Aliquots of the sample were withdrawn at 60 min, 3 h, 3 days, 5 days and 7 days, and analyzed by ITLC and HPLC.

2.8. Biodistribution studies

All animal experiments were carried out in compliance to European and Greek regulations. Female athymic SCID mice (average weight 20 g, 5 weeks) as well as normal Swiss mice were obtained from the breeding facilities of the NCSR 'Demokritos'. The animals were kept under aseptic conditions until the day of biodistribution.

The SCID mice were inoculated subcutaneously into the right front leg with M165 cells (1×10^7 cells/animal) in 100 μL fetal bovine serum-free medium. When tumors reached a size of 0.2 to 1 g (i.e., 10 to 15 days), biodistribution studies were performed. Tumor-bearing mice were injected via the tail vein with 100 μL of radiotracer [270 kBq/100 μg or 0.4 TBq/mmol (10.94 Ci/mmol)]. Groups of three animals were sacrificed at 4, 24, 48 and 168 h after injection of radiolabeled antibody. To determine VEGF-A specificity, an excess of unlabeled bevacizumab (100-fold) was injected 24 h prior to the injection of the ^{95}Nb-Df-bevacizumab. Blocking studies were performed at 24 and 48 h p.i.

Biodistribution studies of ^{95}Nb-Df, ^{95}Nb-chloride and ^{95}Nb-oxalate were performed in healthy mice. Each animal received an injection of 100 μL of radiotracer [300 kBq/~10 μg or 4.5 TBq/mmol (121,56 Ci/mmol)]. Groups of three animals were sacrificed at 4, 24, 48 and 168 h after injection of the compounds.

Tumors (in the case of SCID mice), tissues and organs (blood, heart, liver, stomach, intestines, spleen, muscle, lungs, pancreas, muscle and bones) were excised, blotted dry and weighed. Samples were counted in a gamma counter (NaI gamma counter, Packard). Standards were prepared from the injected material and were counted each time simultaneously with the tissues excised, allowing for calculations to be corrected for physical decay of the radioisotope. Radiolabeled antibody distribution over time was expressed as injected dose per gram (%ID/g).

2.9. PET imaging studies

PET imaging was performed on an experimental, small field-of-view PET camera, designed and assembled by the "Detector and Imaging Group" of the "Thomas Jefferson National Accelerator Facility, USA, in collaboration with the Department of Biomedical Engineering of the Technological Educational Institute of Athens. The high performance of the system is achieved by using the very fast LSO crystal with 2.5 × 2.5 × 15 mm^3 pixels, the Hamamatsu H8500 PSPMTs, fast amplification electronics, an FPGA system and USB 2 data transfer protocol. Image reconstruction is performed with JAVA in the Kmax environment. The field of view of the system is 50 × 50 mm^2, thus it allows only part of the mouse to be imaged in one position and the spatial resolution has been found equal to 3 mm in coincidence mode. Static images were recorded.

Tumor-bearing SCID mice were injected with 200 kBq/100 μg of ^{90}Nb-bevacizumab (0.3 TBq/mmol or 8.1 Ci/mmol) volume 100 μL and were anesthetized by i.p. injection of 100 μl/10 g mouse body weight of a cocktail solution of ketamine/xylazine (Imalgene, 100 mg/ml, Merial, France and Rompun, 20 mg/ml, Bayer, Germany, respectively).

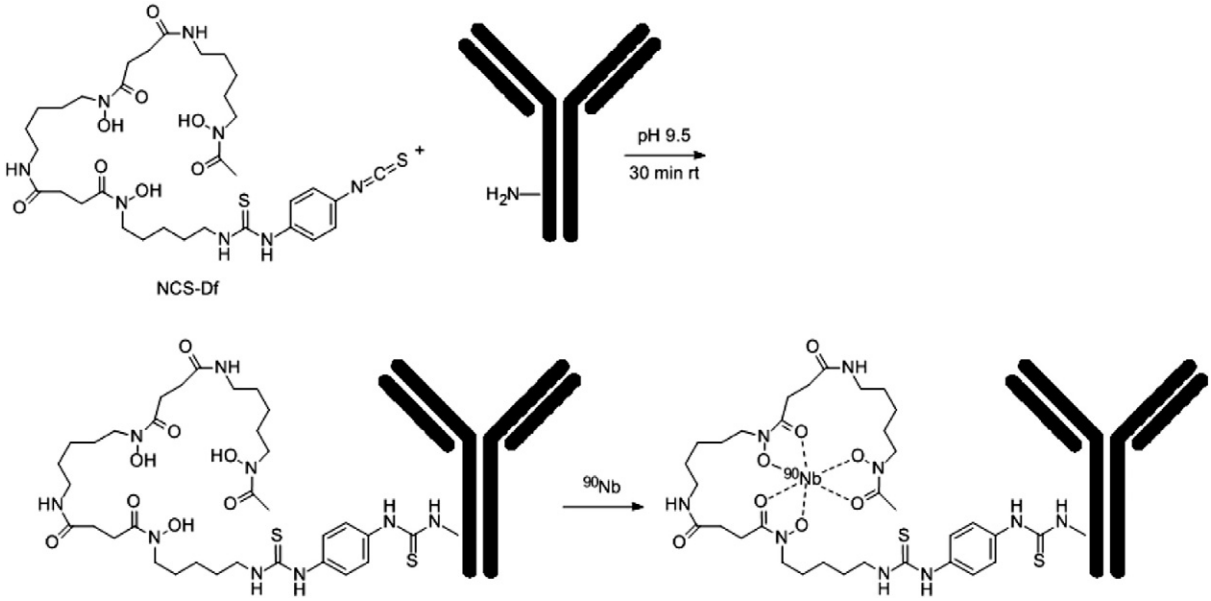

Fig. 1. Df-conjugation of the monoclonal antibody *via* NCS-Bz-Df and labeling with $^{95/90}$Nb (not proven by crystal structure).

3. Results

3.1. Production of $^{95/90}$Nb

3.1.1. ^{90}Nb

The overall irradiation yield of ^{90}Nb for three 1 h and 5 μA irradiations was 720 ± 50 MBq, i.e., 145 ± 10 MBq/μAh under given irradiation parameters. The radionuclidic purity of ^{90}Nb after EOB was more than 97%. Minor isotopic impurities found were: ^{92m}Nb ($T_{1/2}$ = 10.2 days) = 1.64%, ^{95}Nb ($T_{1/2}$ = 35.0 days) = 0.08%, ^{95m}Nb ($T_{1/2}$ = 3.6 days) = 0.29% and ^{96}Nb ($T_{1/2}$ = 23.35 h) = 0.88%. The calculated theoretical specific activity for ^{90}Nb is $8.9 \cdot 10^7$ GBq/g.

3.1.2. ^{95}Nb

At a neutron flux of $2 \cdot 10^{14}\ s^{-1} \cdot cm^{-2}$ (BER II), a 50-day irradiation of 300 mg target produced more than 1.5 GBq of ^{95}Zr. The maximum daughter activity of ^{95}Nb generated from ^{95}Zr was obtained at ~67 days, EOB. The calculated theoretical specific activity for ^{95}Nb is $1.4 \cdot 10^6$ GBq/g.

3.2. Separation and purification of no-carrier added $^{95/90}$Nb

3.2.1. First separation strategy

The extraction steps provided crude separation of $^{95/90}$Nb from the target material with the organic phase collecting more than 99% of $^{95/90}$Nb. After the back extraction procedure, the 5 mL aqueous phase contained 90–95% of the $^{95/90}$Nb activity. After both extractions this corresponds to a high reduction of the Zr target mass by a factor of 10^4. Subsequent anionic exchange separation further removes those traces of Zr. The final separation yield of $^{95/90}$Nb was 60–65% and the decontamination factor for Zr/Nb was ≥10^7, representing ≤26 ng of Zr present in the final $^{95/90}$Nb fraction. The separation was performed for each niobium isotope separately.

3.2.2. Second separation strategy

The overall separation proceeds with a yield of 93–95% of $^{95/90}$Nb, collected in 400 μL 0.1 M oxalic acid. The whole separation procedure takes less than one hour, which is almost 4 times faster than the first separation method. The decontamination after UTEVA purification is 3×10^8. This decontamination factor equals 0.77 ng of zirconium present in the final fraction for a 260 mg zirconium target.

3.3. Preparation of $^{95/90}$Nb-labeled Df-Bz-NCS-mAb

The ^{90}Nb labeling yield was >90% (96% ITLC, 95% HPLC) after 1 h. Labeling kinetics indicate that the labeling yields reached ≥80% already at 15 min and increased to more than 90% after 50 min. After SEC separation on a PD-10 column, the ^{90}Nb-Df-mAb derivative had 99.0% purity, cf. Fig. 2. The specific activity of $^{95/90}$Nb-bevacizumab labeled with the ^{95}Nb from the first separation strategy was 0.4 TBq/mmol (10.94 Ci/mmol), while from the alternative separation strategy, the specific activity of the radiotracer was 4.5 TBq/mmol (121.56 Ci/mmol).

3.4. In vitro stability

After 3 days of incubation in saline at room temperature, more than 99% (≥99% HPLC, ≥99% ITLC) and after 7 days ≥95% (99% HPLC, 97% ITLC) of $^{95/90}$Nb-Df-Bevacizumab were detected. Stability testing in fresh human plasma at 37 °C showed only slightly higher product degradation, cf. Fig. 3. After 3 days of incubation ≥94% (97% HPLC, 94% ITLC) of labeled product was available, while at 7 days ≥86% (89% HPLC, 86% ITLC) of the product was still intact.

3.5. Biodistribution experiments

3.5.1. Biodistribution of ^{95}Nb-oxalate, ^{95}Nb-chloride and ^{95}Nb-Df in healthy mice

TLC results showed quantitative formation (≥ 99%) of ^{95}Nb-Df. The biodistribution of ^{95}Nb-oxalate and ^{95}Nb-chloride showed similar results, with no specific organ uptake observed (Fig. 4). However, for ^{95}Nb-chloride the uptake in all organs was higher in comparison to ^{95}Nb-oxalate. The main uptake was in the blood, lungs and bones. Slight bone accumulation was measured for both substances. Uptake for liver, kidneys and spleen was approximately 1% at 24 h p.i. for oxalate and below 3% for the chloro species. After 168 h p. i. all organs uptakes except for bone were below 1% and 2% respectively, for both ^{95}Nb-oxalate and ^{95}Nb-chloride, apart from the bone uptake, which was ≥2% for the oxalate and ≥4% for the chloride species. ^{95}Nb-Df showed a very fast clearance from the body (Fig. 5). At 24 h p.i., no single organ uptake above 0.5% was observed. After 4 h, uptake in kidneys, stomach and intestines was still detected, while uptake in all other organs was almost negligible. After 168 h p.i. the radiolabeled products had almost completely cleared from the organism.

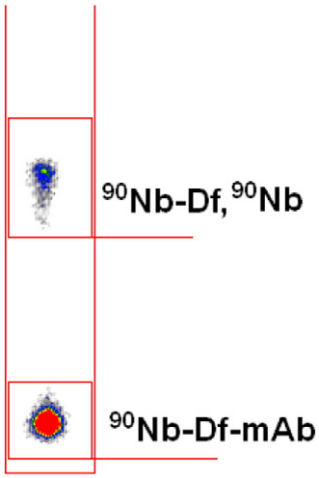

Fig. 2. ITLC image of quantification of labeling efficiency for ^{90}Nb-Df-bevacizumab after 60 min of reaction. Stationary phase: paper impregnated chromatography strip, mobile: phase, 0.02 M citrate buffer (pH 5.0).

3.5.2. Biodistribution of ^{95}Nb-Df-bevacizumab of two different specific activities in tumor-bearing and healthy mice

Biodistribution of ^{95}Nb-Df-bevacizumab at an injected dose of 270 kBq/100 μg/mouse (0.4 TBq/mmol or 10.94 Ci/mmol) showed a relatively low accumulation in the tumor (≤3%) at 24 h p.i., which decreased in time (Fig. 5). On the other hand, high accumulation in the liver (>30%), spleen (>10%) and kidneys (>5%) was detected. Indicative blocking studies performed at two time-points (24 and 48 h p.i.) showed that VEGF was significantly blocked when an excess amount of bevacizumab (100-fold) was injected 24 h prior to the injection of the radiotracer, thus showing the specificity of ^{95}Nb-bevacizumab binding to the VEGF-positive tumor (24 h p.i.: 2.77 ± 1.07%ID/g *vs* 1.07 ± 0.37%ID/g, $p < 0.01$; 48 h p.i.: 1.57 ± 0.57%ID/g *vs* 0.62 ± 0.29%ID/g, $p < 0.03$).

To prove that the previous biodistribution data, i.e., high liver, lung and spleen uptake, were a consequence of the antibody concentration, i.e., the specific activity of the ^{95}Nb-Df-bevacizumab batch injected and not of the instability of the labeled product, another biodistribution study was conducted, where normal Swiss mice were injected with a higher specific activity product [4.5 TBq/mmol (121.56 Ci/mmol)].

The results presented in Fig. 6 show a different kinetic behavior for the higher specific activity of ^{95}Nb-Df-bevacizumab. Significantly less uptake in the liver (3.32 ± 0.28% ID/g *vs* 33.33 ± 4.83% ID/g, $p < 0.0002$), as well as in the spleen (2.24 ± 0.29% ID/g *vs* 12.47 ± 3.70% ID/g, $p < 0.004$) was observed at 24 h p.i. for the higher-specific-activity radiotracer, which further rapidly decreased over time. After 168 h, the uptake in these organs was less than 2%. On the other hand, a much higher initial uptake in blood (13.02 ± 1.13% ID/g *vs* 1.68 ± 0.44% ID/g, $p < 0.00004$) and lungs (5.96 ± 0.12% ID/g *vs* 1.43 ± 0.95% ID/g, $p < 0.0006$) was detected. At 168 h p.i., the uptake in these organs is significantly decreased as well (6.96 ± 1.53% ID/g *vs* 13.02 ± 1.13% ID/g, $p < 0.003$ and 2.70 ± 0.82% ID/g *vs* 5.96 ± 0.12% ID/g, $p < 0.001$ for blood and lung at 168 h and 24 h p.i., respectively). Significant tracer uptake was observed in the heart, which can be attributed to high blood uptake levels. A constant bone uptake (approx. 2% ID/g) was observed over the range of 4 to 168 h, thus allowing us to conclude that no release of ^{95}Nb from the labeled monoclonal antibody occurs.

3.5.2.1. PET imaging of ^{95}Nb-Df-bevacizumab in tumor-bearing mice. Static PET imaging was performed on an experimental small animal PET camera (Fig. 7). Due to the low specific activity of ^{90}Nb-Df-bevacizumab, a single PET image only was obtained at 4 h post-injection. However, even at this early time-point, the tumor is clearly delineated, while there is noticeable accumulation of the radiotracer in the heart, liver and lung areas, as is expected from the ^{95}Nb-Df-bevacizumab biodistribution results at 4 h p.i. These data provide the first image of a ^{90}Nb-labeled monoclonal antibody described in literature.

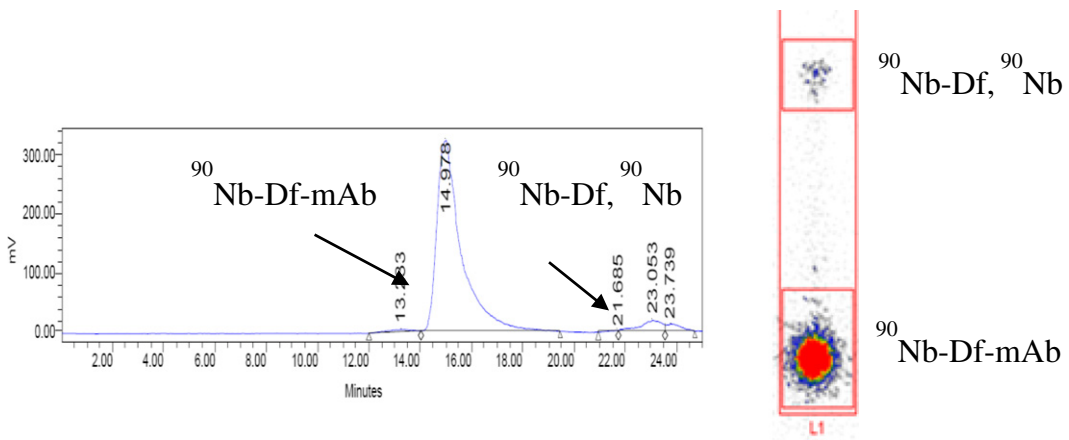

Fig. 3. ITLC image (right) and HPLC chromatogram (left) of *in vitro* stability ^{90}Nb-Df-bevacizumab after 7 days in saline at room temperature. ITLC: Stationary phase: paper impregnated chromatography strip mobile: phase, 0.02 M citrate buffer (pH 5.0), HPLC: Waters HPLC system using a TSKgel G3000SWXL size exclusion column (TOSOH Bioscience, Germany). As eluent, a mixture of 0.05 M sodium phosphate and 0.15 M sodium chloride solution (pH 6.8) was used at a flow rate of 0.8 mL/min.

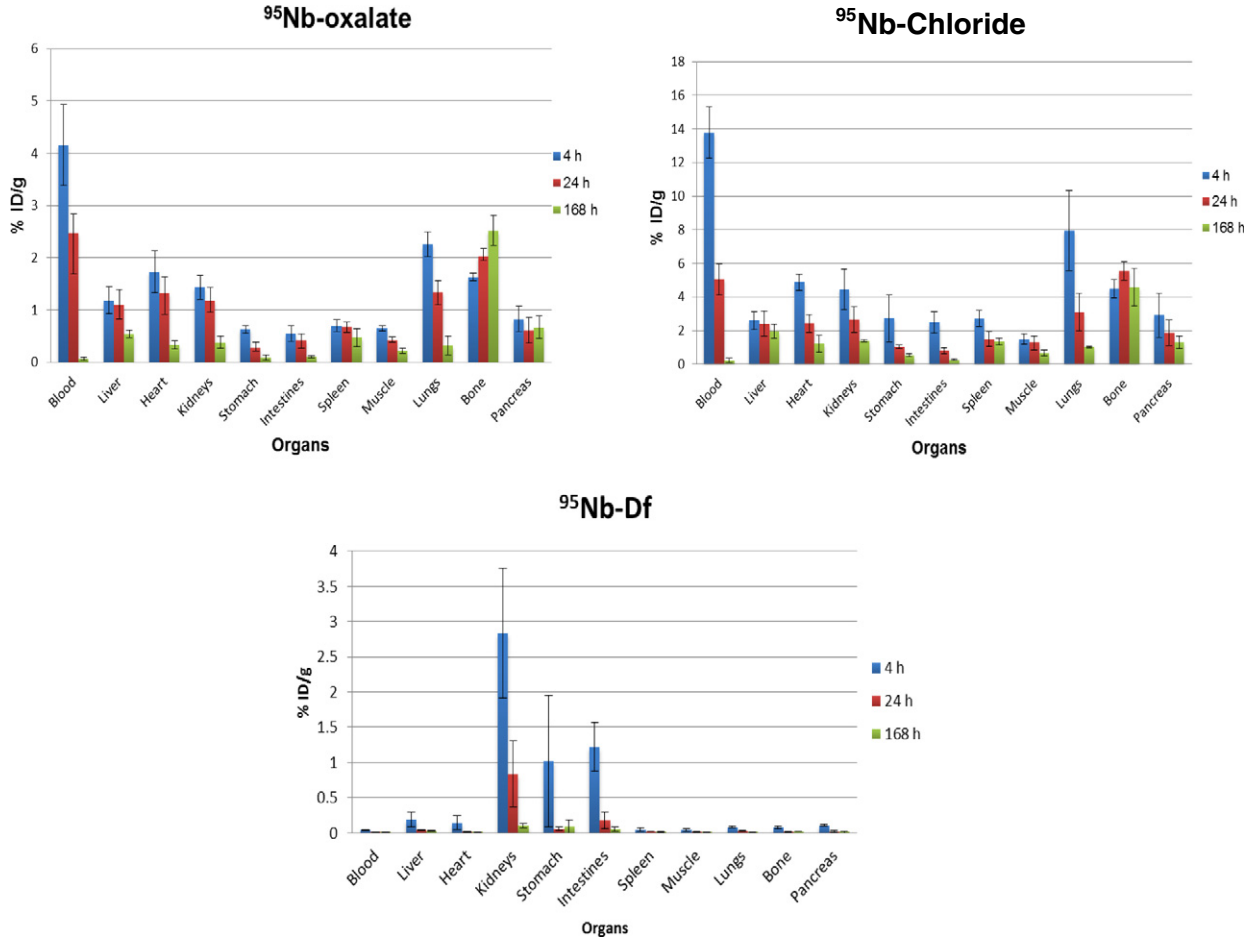

Fig. 4. Biodistribution of ^{95}Nb-oxalate, ^{95}Nb-chloride and ^{95}Nb-Df in healthy mice.

4. Discussion

The radiolabeled monoclonal antibody ^{95}Nb-Df-bevacizumab with a maximal specific activity of 0.4 TBq/mmol (10.94 Ci/mmol) was synthesized during the first separation strategy which is described herein. Our alternative separation strategy provided more than 10 times higher specific activity [4.5 TBq/mmol (121,56 Ci/mmol)] for ^{95}Nb and even higher for ^{90}Nb (~45 TBq/mmol (1216 Ci/mmol).

This study aimed at first evaluations of a ^{90}Nb-labeled monoclonal antibody. While both isotope production and labeling appear to be established, the data on the *in vitro* stability of the proof-of-principle ^{95}Nb-Df-bevacizumab have been obtained for the first time. It can be

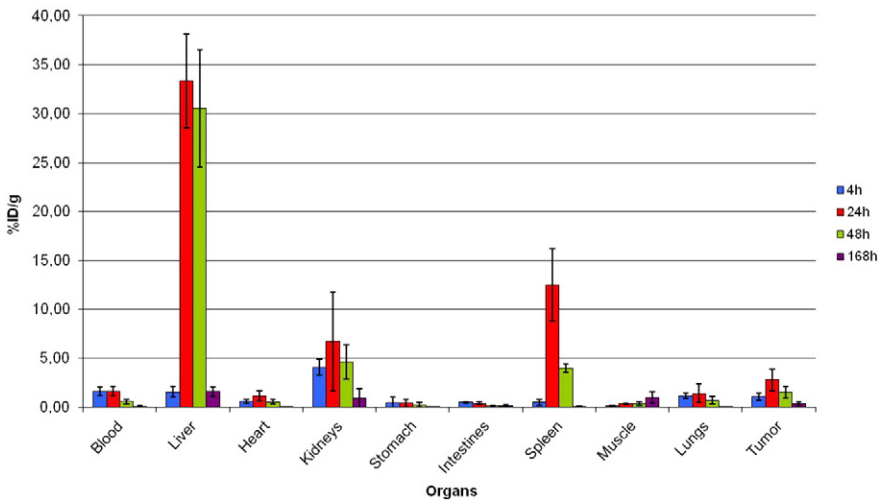

Fig. 5. Biodistribution of low specific activity 0.4 TBq/mmol (10.94 Ci/mmol) of ^{95}Nb-Df-bevacizumab in tumor-bearing mice.

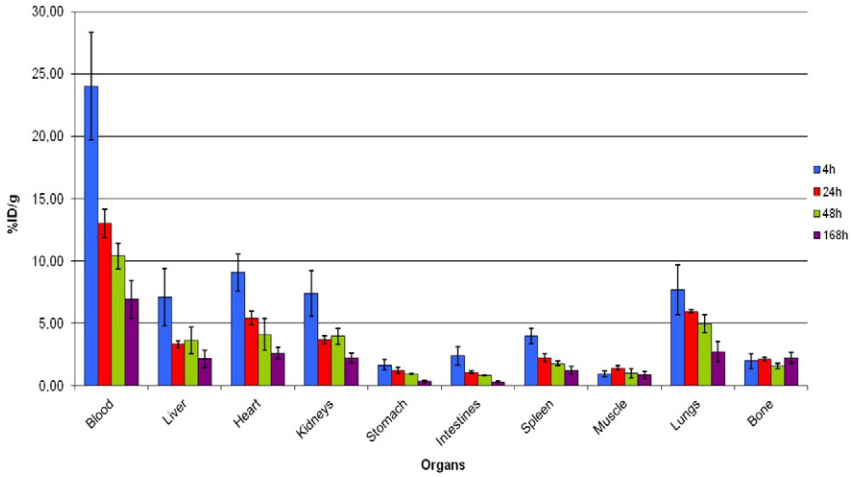

Fig. 6. Biodistribution of high specific activity 4.5 TBq/mmol (121.56 mCi/mmol) of ^{95}Nb-Df-bevacizumab in normal Swiss mice.

concluded, that the Df-mediated label is stable *in vitro*. *In vivo* experiments showed the same result, where ^{90}Nb-data *in vivo* match ^{95}Nb-data from *in vitro* studies.

However, the pharmacology of the two radiotracers clearly depended on the specific activity of the ^{90}Nb-labeled monoclonal antibody, revealing significant accumulation in non-tumor organs.

Consequently, the separation chemistry of radioniobium from both nuclear reactor (^{95}Nb) and cyclotron (^{90}Nb) irradiated zirconium targets was improved. This allowed the synthesis of *Nb-Df-bevacizumab batches of significantly increased specific activity, which is comparable to the specific activity of bevacizumab radiolabeled with other isotopes, as shown by various groups [e.g. Nagengast et al. [3] reported specific activities of 8.7 TBq/mmol (235.14 Ci/mmol) and 7.5 TBq/mmol (202.7 Ci/mmol) for ^{89}Zr-bevacizumab and ^{111}In-bevacizumab, respectively, while Paudyal et al. [4] acquired specific activities of 0.38–0.6 TBq/mmol (10.2–16.2 Ci/mmol) for ^{64}Cu-bevacizumab].

Biodistribution of 100 μg of bevacizumab with our lower specific activity of ^{95}Nb-Df-bevacizumab (0.4 TBq/mmol) showed adequate tumor uptake (3%), with tumor-to-blood ratios of 1.65 and 3.64 at 24 and 168 h p.i. respectively, which are comparable to the results of Nagengast et al., for ^{89}Zr-bevacizumab (T/B ratios of 0.51 and 1.86 at 24 and 168 h p.i. respectively), and other groups [3,4]. The significant difference which was observed was the unusually high uptake in liver, spleen and kidneys at 24 h p.i. The first image of a ^{90}Nb-labeled antibody was also acquired on an experimental small animal PET camera, which was in good agreement to our *ex vivo* biodistribution studies, i.e., even though the acquired images need refining, satisfactory tumor and enhanced liver uptake can be observed.

To prove that liver and spleen uptake is the result of low specific activity radiolabeled antibody, an *in vivo* evaluation of ^{95}Nb-oxalate, ^{95}Nb-chloride and ^{95}Nb-Df was initially conducted. These compounds can be formed by destruction of the labeled product. Biodistribution of these compounds in healthy mice did not show specific uptake in any organs. The concentration of ^{95}Nb-chloride and ^{95}Nb-oxalate in the blood remained high up to 24 h p.i., which can probably be attributed to the formation of metal complexes with plasma proteins [19,20]. A relatively high uptake in the heart and lung, both highly-vascularized organs, is also observed up to 24 h p.i. This activity was rapidly cleared in favor of uptake in the bone. The bone uptake for both ^{95}Nb-chloride and ^{95}Nb-oxalate demonstrates the high affinity of $Nb^{(V)}$ to phosphonate, which is so strong that, in the case of ^{95}Nb-oxalate it shows a slow but steady increase in percentage of bone uptake, while for ^{95}Nb-chloride a small decrease in bone uptake is observed. ^{95}Nb-Df was immediately cleared from the system, without any sign of bone uptake.

The final step in this work was to evaluate a higher specific activity sample of ^{95}Nb-bevacizumab in healthy mice. These results showed pronounced uptake in the blood, heart and lungs, which diminished at 24 h p.i., while uptake in the liver, spleen and kidneys, as well as in bone, was low. These data clearly prove the high *in vivo* stability of Nb-Df-conjugated biomolecules.

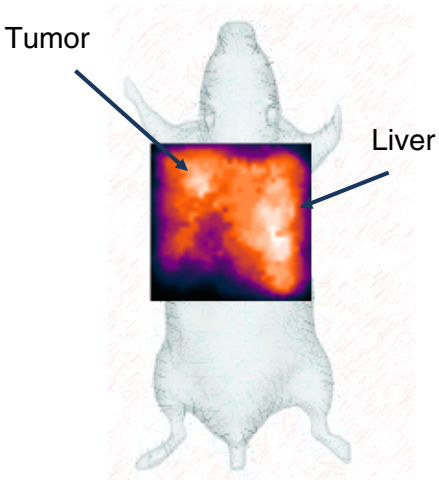

Fig. 7. Static PET imaging 4 h p.i. of ^{90}Nb-Df-bevacizumab. The mouse was injected with 200 kBq/100 μg of ^{90}Nb-bevacizumab (volume 100 μL) and anesthetized by i.p. injection of 100 μl/10 g mouse body weight of a cocktail solution of ketamine/xylazine.

5. Conclusions

The obtained results provide a very important proof of stability of $^{95/90}$Nb labeled biomolecules *in vivo*. The radiolabeled monoclonal antibody ^{95}Nb-Df-bevacizumab with a relatively high specific activity (4.5 TBq/mmol (121.56 Ci/mmol) was obtained, which allowed us to conduct biodistribution studies upon injection of a low concentration of bevacizumab (~10 μg/100 μl). The continuation of this project is well-justified, as our results show that there is great promise for the application of ^{90}Nb in *immuno*-PET.

Acknowledgments

The authors gratefully acknowledge financial support from the COST Action TD1004 (Theranostics Imaging and Therapy: An Action to Develop Novel Nanosized Systems for Imaging-Guided Drug Delivery), the Program for the Promotion of the Exchange and Scientific Cooperation between Greece and Germany IKYDA, scientific project titled "Targeted *Immuno*-PET imaging of neoangiogenesis with biomolecules labeled with the positron-emitter Niobium-90" (Contract number 205), the German Research Foundation under DFO Ro 985/40-1 and Russian Foundation for Fundamental Research grant (RFBR 15-53-12372).

We would also like to thank the teams of BR2 and TRIGA Mainz reactors for production of the Niobium isotopes.

References

[1] Rösch F, Baum RP. Generator-based PET radiopharmaceuticals for molecular imaging of tumours: on the way to THERANOSTICS. Dalton Trans 2011;40(23):6104–11.
[2] Ellis LM, Hicklin DJ. VEGF-targeted therapy: mechanisms of anti-tumour activity. Nat Rev Cancer 2008;8:579–91.
[3] Nagengast WB, de Vries EG, Hospers GA, Mulder NH, de Jong JR, Hollema H, et al. In vivo VEGF imaging with radiolabeled bevacizumab in a human ovarian tumor xenograft. J Nucl Med 2007;48:1313–9.
[4] Paudyal B, Paudyal P, Noboru O, Hanaoka H, Tominaga H, Endo K. Positron emission tomography and biodistribution of vascular endothelial growth factor with ^{64}Cu-labeled bevacizumab in colorectal cancer xenografts. Cancer Sci 2011;201(1):117–21.
[5] Nagengast WB, de Korte MA, Oude Munnink TH, Timmer-Bosscha H, den Dunnen WF, Hollema H, et al. ^{89}Zr-bevacizumab PET of early antiangiogenic tumor response to treatment with HSP90 inhibitor NVP-AUY922. J Nucl Med 2010;51:761–7.
[6] Nayak TK, Garmestani K, Baidoo KE, Milenic DE, Brechbiel MW. PET imaging of tumor angiogenesis in mice with VEGF-A-targeted ^{86}Y-chx-a″-dtpa-bevacizumab. Int J Cancer 2011;128:920–6.
[7] Chang AJ, Sohn R, Lu ZH, Arbeit JM, Lapi SE. Detection of rapalog-mediated therapeutic response in renal cancer xenografts using ^{64}Cu-bevacizumab immunoPET. 2013;8(3):e58949.
[8] Vugts DJ, Visser GW, van Dongen GA. ^{89}Zr-PET radiochemistry in the development and application of therapeutic monoclonal antibodies and other biologicals. Curr Top Med Chem 2013;13(4):446–57.
[9] Severin GW, Engle JW, Barnhart TE, Nickles RJ. 89Zr radiochemistry for positron emission tomography. Med Chem 2011;7(5):389–94.
[10] Anderson CJ, Ferdani R. Copper-64 radiopharmaceuticals for PET imaging of cancer: advances in preclinical and clinical research. Cancer Biother Radiopharm 2009;24(4):379–93.
[11] Rosch F, Herzog H, Stolz B, Brockmann J, Kohle M, Muhlensiepen H, et al. Uptake kinetics of the somatostatin receptor ligand [^{86}Y]DOTA-DPHE1-TYR3-octreotide ([^{86}Y]smt487) using positron emission tomography in non-human primates and calculation of. Med Mol Imag 2003;30:510–8.
[12] Nayak TK, Brechbiel MW. ^{86}Y based PET radiopharmaceuticals: radiochemistry and biological applications. Med Chem 2011 Sep;7(5):380–8.
[13] Tolmachev V. Radiobromine-labelled tracers for positron emission tomography: possibilities and pitfalls. Curr Radiopharm 2011;4(2):76–89.
[14] Busse S, Brockmann J, Roesch F. Radiochemical separation of no-carrier-added radioniobium from zirconium targets for application of ^{90}Nb-labelled compounds. Radiochim Acta 2002;90:411–5.
[15] Radchenko V, Filosofov DV, Bochko OK, Lebedev NA, Rakhimov A, Aksenov NV, et al. Separation of ^{90}Nb from zirconium target for application in *immuno*-PET. Radiochim Acta 2014;102(5):433–43.
[16] Radchenko V, Hauser H, Eisenhut M, Vugts JD, van Dongen GAMS, Roesch F. ^{90}Nb — a potential PET nuclide: production and labeling of monoclonal antibodies. Radiochim Acta 2012;100(11):857–63.
[17] Radchenko V, Busse S, Roesch F. Desferrioxamine as an appropriate chelator for ^{90}Nb: comparison of its complexation properties for M-Df-octreotide (M = Nb, Fe, Ga, Zr). Nucl Med Biol 2014;41(9):721–7.
[18] Perk LR, Vosjan MJ, Visser GW, Budde M, Jurek P, Kiefer GE, et al. *p*-sothiocyanatobenzyl-desferrioxamine: a new bifunctional chelate for facile radiolabeling of monoclonal antibodies with zirconium-89 for immuno-PET imaging. Eur J Nucl Med Mol Imaging 2009;37:250–9.
[19] Mealy J. Turn-over of carrier-free zirconium in man. Nature 1957;179:673–4.
[20] Backstrom J, Hammarstrom L, Nelson A. Distribution of zirconium and niobium in mice: autoradiographic study. Acta Radiol Diagn 1967;6(2):122–8.